HHS Public Access

Author manuscript

Nat Struct Mol Biol. Author manuscript; available in PMC 2012 March 01.

Published in final edited form as:

Nat Struct Mol Biol. ; 18(9): 999–1005. doi:10.1038/nsmb.2095.

An Autoinhibitory Helix in the C-Terminal Region of Phospholipase C-β Mediates $G\alpha_q$ Activation

Angeline M. Lyon[1], **Valerie M. Tesmer**[1], **Vishan D. Dhamsania**[1], **David M. Thal**[1], **Joanne Gutierrez**[3], **Shoaib Chowdhury**[3], **Krishna C. Suddala**[2], **John K. Northup**[3], and **John J. G. Tesmer**[1,4]

[1]Life Sciences Institute, University of Michigan, 210 Washtenaw Avenue, Ann Arbor, MI 48109-2216, USA

[2]Department of Biophysics, University of Michigan, 210 Washtenaw Avenue, Ann Arbor, MI 48109, USA

[3]Laboratory of Cell Biology, National Institute on Deafness and Other Communication Disorders, National Institutes of Health, 5 Research Court, Rockville, MD 20850, USA

[4]Department of Pharmacology, University of Michigan, 1150 W. Medical Center Drive, Ann Arbor, MI 48109-5632, USA

Abstract

Phospholipase C-β (PLCβ) is a key regulator of intracellular calcium levels whose activity is controlled by heptahelical receptors that couple to G_q. We have determined atomic structures of two invertebrate homologs of PLCβ (PLC21) from cephalopod retina and identified a helix from the C-terminal regulatory region that interacts with a conserved surface of the catalytic core of the enzyme. Mutations designed to disrupt the analogous interaction in human PLCβ3 dramatically increase basal activity and diminish stimulation by $G\alpha_q$. $G\alpha_q$ binding requires displacement of the autoinhibitory helix from the catalytic core, thus providing an allosteric mechanism for activation of PLCβ.

Phospholipase C-β (PLCβ) proteins form a highly conserved enzyme family that hydrolyze phosphatidylinositol 4,5-bisphosphate (PIP_2) into inositol-1,4,5-triphosphate (IP_3) and diacylglycerol, two key second messengers that mobilize intracellular calcium and stimulate the activity of protein kinase C[1,2]. PLCβ isoforms are potently activated via direct interactions with heterotrimeric G proteins of the $G\alpha_q$ family[3,4], Gβγ heterodimers[5–8], and

Correspondence should be addressed to J. T. (tesmerjj@umich.edu) and J.N. (northupj@nidcd.nih.gov).

Accession codes. The *S*PLC21 and *L*PLC21 structures and their structure factor amplitudes are deposited in the Protein Data Bank with accession codes 3RQ0 and 3RQ1, respectively.

AUTHOR CONTRIBUTIONS

A.M.L, V.M.T., J.K.N, and J.J.G.T. designed the overall experimental approach. J.G., S.C., and J.K.N. purified *L*PLC21 and *S*PLC21, and cloned and sequenced cDNA encoding *S*PLC21. K.C.S. crystallized *L*PLC21. A.M.L. crystallized *S*PLC21 and determined the crystal structures of *L*PLC21 and *S*PLC21. A.M.L. and V.M.T. cloned, expressed, and purified human PLCβ3 variants. V.M.T. cloned, expressed, and purified $G\alpha_q$. A.M.L. conducted all activity-based assays. D.M.T helped design and together with V. D. D. conducted ThermoFluor and FCPIA assays. A.M.L, V.M.T., and J.J.G.T co-wrote the manuscript.

small GTPases such as Rac1[9,10]. The interaction between $G\alpha_q$ and PLCβ is of particular interest because regulation of PLCβ by G_q-coupled receptors is critical for normal cardiomyocyte function, and maladaptive changes in this pathway can result in the onset of cardiac arrhythmias, cardiac hypertrophy, and heart failure[11–14].

PLCβ proteins and their invertebrate homologs NorpA[15] and PLC21[16,17] share a highly conserved catalytic core comprised of an N-terminal pleckstrin homology (PH) domain, followed by four EF hand domains, a triose-phosphate isomerase (TIM) barrel-like catalytic domain split into X and Y halves by a variable linker[18,19], and a C2 domain[1,20] (Fig. 1a)[21,22,23]. The X-Y linker is positioned adjacent to the active site, and its cleavage or truncation increases basal activity[22,24,25]. However, such activation is independent of both heterotrimeric G proteins and small GTPases[22]. The distinguishing feature of PLCβ enzymes is a ~400 amino acid C-terminal region (CTR) that is known to be important for membrane association as well as $G\alpha_q$ binding and activation[1,26–29]. Many of these functional properties have been mapped to residues within an extended coiled-coil domain found in the C-terminus, corresponding to residues 946 to 1200 in human PLCβ3 (Fig. 1a)[1,26–29]. Recently, a structure was reported for $G\alpha_q$ in complex with a human PLCβ3 truncation (Δ887) that includes a small portion of the CTR (residues 848 to 882). This region forms a helix-turn-helix motif (Hα1-Hα2) that docks with the effector-binding site of $G\alpha_q$[23]. Although this structure revealed key interactions between PLCβ3 and $G\alpha_q$, the activity of the Δ887 fragment was not shown to be regulated by $G\alpha_q$ and thus it remains unclear how $G\alpha_q$ enhances PLCβ3 activity and how other regions of the CTR contribute to its regulation[27,30,31].

To better understand the activation mechanism of PLCβ, we solved crystal structures of two invertebrate, endogenously expressed PLCβ homologs from cephalopod retina. Within these structures, a helix located immediately C-terminal to the portion of the Hα1-Hα2 motif that directly interacts with $G\alpha_q$ is observed to dock with a conserved cleft on the PLCβ catalytic core. Perturbation of the analogous interaction in human PLCβ3 dramatically enhances basal activity, lowers the thermostability of the enzyme, increases $G\alpha_q$ affinity, and reduces the efficacy of $G\alpha_q$ activation. Our results are consistent with an allosteric mechanism in which $G\alpha_q$ binding displaces this inhibitory helix, leading to enhanced activity. Our studies also confirm that more distal regions of the CTR enhance the affinity of PLCβ3 for $G\alpha_q$ and facilitate PIP_2 hydrolysis through a mechanism independent of $G\alpha_q$.

RESULTS

Structures of cephalopod PLC21

Crystal structures of endogenously expressed *Loligo pealei* (*L*PLC21) and *Sepia officinales* PLC21 (*S*PLC21) were solved by molecular replacment to 3.1 and 2.0 Å resolution, respectively (Fig. 1b,c and Table 1). For this work, it was necessary to sequence the coding region for *S*PLC21 from its endogenous source, which we found to be ~92% identical to that of *L*PLC21. Although full length proteins were subjected to crystallization trials, both *S*PLC21 and *L*PLC21 crystallized as ~95 kDa proteolytic fragments (Supplementary Methods online) that contain visible density for most of the catalytic core. In the higher resolution *S*PLC21 structure, residues 11–474 and 485–774 of the catalytic core as well as

26 residues from the CTR (residues 790–815) are visible. The catalytic cores of *L*PLC21 and *S*PLC21 are essentially identical, and superimpose with an r.m.s.d. value of 0.36 Å for 765 Cα atoms (out of 778 total in *S*PLC21). Within the catalytic core of *S*PLC21, only a short segment of the X-Y linker (amino acids 475–484) is missing electron density (Supplementary Fig. 1 online). There are only subtle differences in the domain arrangment of the catalytic core between cephalopod and human homologs. Most notably, the EF hand and C2 domains of *S*PLC21 are rotated by ~6° away from the TIM barrel and PH domains relative to their positions in the structures of PLCβ2 and PLCβ3.

The TIM barrel-like domain of *S*PLC21 is ~55% identical in sequence with those of human PLCβ2 and PLCβ3, and can be superimposed with r.m.s.d. values of 0.38 and 0.39 Å for 232 and 234 Cα atoms, respectively, omitting the X–Y linker (residues 473–510 of *S*PLC21). In *S*PLC21, the C-terminal end of the linker (residues 500–510, corresponding to residues 576–586 in human PLCβ3) has essentially the same structure as in other PLCβ structures. However, residues 485–499 form a helix that extends from the catalytic site in a different direction than observed in previous PLCβ structures (Supplementary Fig. 1 online) [22,23]. The signficance of this difference is not yet understood, but this unique conformation is also found in both unique chains of *L*PLC21 (Fig. 1b) suggesting that it is not dictated by the crystal packing environment.

In both PLC21 structures, strong electron density is observed for a segment of the CTR that can be modeled as a helical hairpin composed of Hα2′ and Hα3 helices (residues 790–816 of *S*PLC21) (Fig. 2a,b and Supplementary Fig. 2 online). The loop connecting the hairpin to the end of the C2 domain (residues 775–789) is disordered. The Hα2′ helix (residues 792–805) corresponds to the C-terminal end of the PLCβ3 Hα2 helix, just beyond the region of the Hα1-Hα2 motif in PLCβ3 that directly contacts $G\alpha_q$ (Fig. 1d and Supplementary Fig. 3a online). Hα2′ packs against a highly conserved, hydrophobic cleft formed between the TIM barrel and C2 domains of the catalytic core, in close proximity to the active site and X–Y linker, and buries 1200 $Å^2$ of solvent accessible surface area (Fig. 2a,b). The side chains of Arg797, Leu801, and Phe804 form the principal interactions from Hα2′. The positively-charged guanidinium group of Arg797 caps the C-terminus of the Tα5 helix of the TIM barrel domain, and, along with Ala800 and Leu801, forms a hydrophobic pocket for the Phe639 side chain located in the linker between the TIM barrel and C2 domains of the catalytic core. The side chain of Phe804 packs in a hydrophobic cavity formed by the side chains of Val584 and Ile587 in the Tα6 helix of the TIM barrel domain and Pro679 and Thr682 of the C2 domain. The C-terminal end of Hα2′ is capped by the side chain of Arg684 from the C2 domain. The residues involved in these interactions are highly conserved among PLCβ enzymes, but poorly so in other PLC isozymes (Supplementary Fig. 3 online), consistent with the hypothesis that they contribute to a functionally important, PLCβ-specific intramolecular contact. Indeed, the same Hα2′-catalytic core interaction is observed in the *S*PLC21 structure (Fig. 1c and Fig. 2a,c) and the two independent chains of the *L*PLC21 structure (Fig. 1b), and a very similar interaction is formed in the $G\alpha_q$–PLCβ3 crystal structure as an intermolecular crystal contact (Fig. 2c,d). The Hα2′-catalytic core interaction has thus persisted over 500 million years of evolution[32].

$G\alpha_q$ binding to the Hα1-Hα2 motif is incompatible with the Hα2′ helix binding to the catalytic core in the same molecule. Indeed, the region is required to undergo a large conformational change upon $G\alpha_q$ binding, as the Cα atom of PLCβ3-Arg872 is translated ~50 Å away from its position when Hα2′ is docked with the catalytic core, as modeled by the equivalent atom of Arg797 in the *S*PLC21 structure (Fig. 1c,d). Given the high sequence conservation of Hα2′ among PLCβ isoforms, its close proximity to the active site, and its juxtaposition with the primary $G\alpha_q$ binding site, we hypothesized that the Hα2′ helix plays a role in the regulation of PLCβ by $G\alpha_q$. For subsequent experiments, we focused on human PLCβ3 because it is readily expressed in baculovirus-infected insect cells and is potently and efficaciously regulated by $G\alpha_q$[7,33].

The Hα2′ helix modulates stability of the catalytic core

If the Hα2′ helix plays a regulatory role, then it should stably associate with the PLCβ catalytic core in solution. To detect this interaction, we used a ThermoFluor assay to measure the thermostability of three purified recombinant variants: PLCβ3 (which spans residues 10–1234 containing the complete CTR), PLCβ3-Δ892 (which terminates at residue 891 after the proximal CTR region observed in the PLC21 and PLCβ3 crystal structures), and PLCβ3-Δ847 (which terminates at residue 846 and lacks the entire CTR) (Fig. 1a). Whereas PLCβ3 and PLCβ3-Δ892 had a similar melting temperature (T_m) of 43 and 45 °C, respectively, PLCβ3-Δ847 had a markedly lower T_m of 38 °C, suggesting that the presence of the proximal CTR enhances the thermal stability of the catalytic core (Fig. 3a and Supplementary Table 1). We next tested if this thermostabilization could be accounted for by specific residues in the interface of Hα2′ with the catalytic core. Indeed, mutation of six individual residues in the context of the full-length protein (PLCβ3) reduced the T_m to 39–40 °C, similar to that of PLCβ3-Δ847 (Supplementary Table 1). Interface mutations in the background of PLCβ3-Δ892 similarly reduced the melting point by ~5 °C. In contrast to its effects in the context of PLCβ3 and PLCβ3-Δ892, the F715A mutation of PLCβ3-Δ847 did not significantly change thermostability, indicating that mutation of the catalytic core itself does not lead to lower stability. Thus, the higher thermostability exhibited by PLCβ3 and PLCβ3-Δ892 relative to PLCβ3-Δ847 is dependent on a specific interaction between the catalytic core and Hα2′.

The Hα2′ helix is an autoinhibitory element

Given the proximity of the Hα2′ helix to the active site and its contribution to protein stability, we hypothesized that its interactions with the core could influence catalytic activity. Because the CTR coiled-coil domain of PLCβ3 facilitates membrane recruitment of the enzyme to the substrate PIP_2, the role of the Hα2′ helix in catalytic activity is most easily assessed by comparison of the truncations PLCβ3-Δ892 and PLCβ3-Δ847, or of site-directed mutations made in the full-length protein versus wild-type. PLCβ3 has 10-fold higher basal specific activity than PLCβ3-Δ892 (54 *vs*. 4.7 mol IP_3 min^{-1} mol^{-1} PLCβ3, respectively), confirming that residues 892–1234 of the CTR strongly promote catalysis. The PLCβ3-Δ847 variant has 3-fold higher activity than PLCβ3-Δ892 (15 mol IP_3 min^{-1} mol^{-1} PLCβ3), indicating that the presence of the proximal CTR inhibits the basal activity of PLCβ3 (Fig. 3b and Table 2). To confirm that specific interactions of Hα2′ with the catalytic core are responsible for the observed differences in basal activity, we measured the

activities of point mutants within the Hα2′-catalytic core interface of PLCβ3. The L663D, F715A and P755K mutants in the catalytic core enhance basal activity by over an order of magnitude, as do point mutants of interacting residues in Hα2′ (Fig. 3c and Table 2). The conservative F715Y mutation leads to a more modest increase in activity (6-fold). The complimentary results obtained from mutation of residues on either Hα2′ or its binding site on the catalytic core strongly suggest that this interaction serves to repress the basal activity of PLCβ3. Interface mutations made in the background of PLCβ3-Δ892 yield smaller but consistent increases in activity, although these results should be considered along with the fact that the F715A mutation also causes a mild increase in activity in the context of PLCβ3-Δ847 (Table 2). Thus, mutations in the catalytic core itself can increase activity, but these effects are greatly amplified in the context of the full-length protein. The basal activity data of full-length PLCβ3 and the thermostability data are consistent with the interaction of Hα2′ with the catalytic core, thereby trapping the TIM barrel-like domain in a more quiescent state.

The Hα2′ helix and distal CTR modulate the affinity of $G\alpha_q$ for PLCβ3

The intermolecular interaction of the Hα1-Hα2 module with $G\alpha_q$ and the intramolecular interaction of Hα2′ with the catalytic core of PLCβ3 are expected to be competitive. If so, then disrupting the Hα2′-catalytic core interface should enhance the affinity of $G\alpha_q$ for PLCβ3. We used a flow cytometry protein interaction assay (FCPIA)[34,35] to measure binding between $G\alpha_q$ and PLCβ3, in which the binding affinities of unlabeled PLCβ3 and its variants for $G\alpha_q$ are determined by their ability to displace a fluorescently-labeled variant of PLCβ3 from beads (Fig. 3d and Table 3). PLCβ3-Δ847 is unable to bind $G\alpha_q$ at any concentration tested, consistent with the absence of the proximal CTR. Although PLCβ3-Δ892 retains this region, it has nearly two orders of magnitude lower affinity for $G\alpha_q$ (270 nM) than full-length PLCβ3 (6 nM), suggesting that the more distal regions of the CTR contribute key interactions that enhance binding to $G\alpha_q$[1,27]. The affinity of our truncation is consistent with that measured by surface plasmon resonance for the Δ887 truncation used in the crystallographic analysis of the $G\alpha_q$–PLCβ3 complex[23]. However, these same studies indicated that full-length PLCβ3 has a similar binding affinity for $G\alpha_q$. The 6 nM binding constant we measure for full-length PLCβ3 is consistent with previously reported EC_{50} values for $G\alpha_q$ stimulation[36] and the EC_{50} values we report in Table 4.

Mutation of residues in either Hα2′ or in its binding site on the catalytic core in PLCβ3-Δ892 enhances the apparent affinity for $G\alpha_q$ by 10-fold, consistent with competition between binding of the Hα1-Hα2 motif to $G\alpha_q$ and the binding of Hα2′ to the catalytic core. Analogous mutations in the longer PLCβ3 protein also seem to enhance affinity for $G\alpha_q$, but only 2–3-fold, possibly because the more distal regions of the CTR play a compensatory role in binding to $G\alpha_q$ (Fig. 3d and Table 3). Our results are therefore consistent with a model in which $G\alpha_q$ binding to PLCβ3 displaces the proximal CTR from the catalytic core, leading to increases in both $G\alpha_q$ affinity and catalytic activity.

Mutations in the Hα2′-catalytic core interface reduce the efficacy of $G\alpha_q$

The profound enhancement in basal activity observed for variants of PLCβ3 in which the Hα2′-catalytic core interface is disrupted is on the same scale as the activation of wild-type

PLCβ3 by $G\alpha_q$. We hypothesized that if $G\alpha_q$ activates PLCβ3 by displacing the autoinhibitory Hα2′ helix, then $G\alpha_q$ should be less efficacious at activating variants of PLCβ3 in which the Hα2′-catalytic core interface is disrupted. However, because $G\alpha_q$ should still be able to bind these variants (Table 3), residual $G\alpha_q$ activation effects might be observed at the same or lower EC_{50} values as measured for the wild-type proteins.

PLCβ3 is activated by $G\alpha_q$ 20-fold to 1100 mol IP_3 min^{-1} mol^{-1} with an EC_{50} of 3 nM, consistent with the binding affinity we measure for these proteins by FCPIA (Table 3) and with previous studies[7,36–38]. PLCβ3-Δ847, which lacks the proximal CTR, is unresponsive to $G\alpha_q$. However, PLCβ3-Δ892 is activated 7-fold by $G\alpha_q$ to 30 mol IP_3 min^{-1} mol^{-1} (Table 4 and Supplementary Fig. 4 online). Considered along with the crystal structure of the $G\alpha_q$–PLCβ3 complex[23], our data firmly establishes that the proximal CTR region confers regulation by $G\alpha_q$. However, the maximal $G\alpha_q$-stimulated rate of hydrolysis catalyzed by PLCβ3 is 40-fold higher than that of PLCβ3-Δ892. Moreover, $G\alpha_q$ activates PLCβ3-Δ892 with a 30-fold higher EC_{50} (130 nM) than wild-type, consistent with the lower binding affinity of $G\alpha_q$ for PLCβ3-Δ892 we measure by FCPIA (Table 3). This data provides further evidence that the more distal regions of the CTR make important contributions to the activation mechanism by enhancing both the catalytic rate and the affinity for $G\alpha_q$.

In the context of PLCβ3, mutations that disrupt the Hα2′-catalytic core interface are activated to a lesser extent by $G\alpha_q$, with only 2–3 fold effects observed. Although we anticipated a small decrease in EC_{50} for these mutants because of their higher affinity for $G\alpha_q$, this trend was only evident in the background of PLCβ3-Δ892. For PLCβ3 and its variants, the EC_{50} values remained in the low nM range and did not consistently decrease as we had measured in FCPIA (Table 3). Because our direct-binding assay is conducted in the presence of liposomes, these results may reflect the important role of the coiled-coil domain in mediating membrane association[24,27,28,31]. However, we did observe that $G\alpha_q$ has 2–3 higher potency when assayed against Hα2′ interface mutants in the background of PLCβ3-Δ892, which retains only the proximal CTR (Supplementary Fig. 4 online and Table 4).

DISCUSSION

Regulation of PLCβ isoforms is tightly controlled, and aberrations in this pathway or its components are associated with a number of pathophysiological processes, including heart failure[11,13,39,40]. One aspect of this control is their exceptionally low level of basal activity and their profound stimulation by G_q-coupled receptors. Previous studies have shown that deletion of the X–Y linker in a variety of PLC isoforms leads to increased basal activity, presumably because acidic charges in the linker electrostatically block access of PIP_2 to the active site[20,22,24]. It has been proposed that membrane recruitment by activators of PLCβ, including $G\alpha_q$, helps to displace this linker[22,23]. However, most PLCβ isoforms are already at least partially localized to the membrane in their basal state[31,41], and deletion or perturbation of the X–Y linker, although profoundly activating, does not eliminate the ability to be activated by heterotrimeric G proteins in simple transfection assays[22,24]. This suggests that heterotrimeric G proteins can activate PLCβ isoforms through a mechanism that is not entirely reliant on the integrity of the X–Y linker.

Our structures of cephalopod PLC21 and functional studies of human PLCβ3 demonstrate that the Hα2′ helix in the proximal CTR interacts with a conserved cleft in the catalytic core. Disrupting the interactions of Hα2′ with the catalytic core dramatically increases basal activity up to ~50 fold (Table 2). The mechanism by which this occurs is as of yet unclear, but is possibly linked to the fact that Hα2′ is positioned on the same side of the TIM barrel as the X–Y linker, which may inhibit basal activity by sterically hindering the interaction of the active site with phospholipid bilayers. Alternatively, decreased thermal stability of the highly active mutants (Supplementary Table 1) implies greater dynamics in the catalytic core, which may lead to enhanced catalysis [42,43]. A third possibility is that Hα2′ exerts a direct negative allosteric effect on the TIM barrel domain itself, although this seems less likely because the catalytic core has essentially the same structure with and without the bound Hα2′ element, as can be seen by comparing structures of PLCβ2 with that of PLCβ3 in the $G\alpha_q$–PLCβ3 complex. Although these structural elements are in close proximity (Fig. 2), a direct functional relationship between displacement of Hα2′ and inhibition imposed by the X–Y linker remains to be explored, but one hypothesis is that disruption of either element leads to a less stable yet more dynamic enzyme with an active site that has easier access to its phospholipid substrates.

We also provide substantial evidence to support an allosteric mechanism by which $G\alpha_q$ modulates the interactions of the Hα2′ helix to activate PLCβ. In the absence of G_q-coupled receptor stimulation, the Hα2′ helix is bound to the catalytic core and suppresses basal activity (Fig. 2a,b and Fig. 3b,c). Our structures of PLC21 indicate that the residues in the Hα1-Hα2 motif that bind $G\alpha_q$ are disordered in this basal state and thus freely accessible to $G\alpha_q$·GTP. $G\alpha_q$·GTP binding to the Hα1-Hα2 motif leads to displacement of the Hα2′ helix from the catalytic core (***cf***. Fig. 1c and Fig. 1d) and dramatically enhanced PIP_2 hydrolysis. Accordingly, disruption of the Hα2′-catalytic core interface by truncation or by site-directed mutagenesis also leads to a marked increase in basal activity (Fig. 3b,c and Table 2) at the expense of $G\alpha_q$ efficacy (Supplementary Fig. 4 and Table 4). However, even in these cases, $G\alpha_q$ binding still activates by ~3-fold, perhaps by increasing the affinity of the catalytic core for phospholipid membranes, or, more generally, by stabilizing a more catalytically competent state. Because our *in vitro* assays used $G\alpha_q$ isolated from the soluble fraction of cell lysates, this residual activation is unlikely to represent enhanced liposome association due to palmitoylation of the N-terminus of $G\alpha_q$.

Our data also strongly indicate that the more distal regions of the CTR contribute to high affinity $G\alpha_q$ binding and to basal and $G\alpha_q$-stimulated activity (Fig. 3b,c,d and Table 4), as has been suggested by many other studies[26,27,29,31,44]. The coiled-coil domain in the CTR contains conserved basic regions important for function[26,27], and plays a role in increasing the affinity of PLCβ for the cell membrane[27,31]. Residues in the coiled-coil domain have also been shown to be important for $G\alpha_q$ activation[26,29,31], and our studies show that the distal CTR enhances the affinity of PLCβ3 for $G\alpha_q$ in protein binding assays conducted in the absence of phospholipid vesicles. The fact that the binding affinities of $G\alpha_q$ for PLCβ3 and PLCβ3-Δ892 (Table 3) are consistent with their respective EC_{50} values measured in our liposome-based hydrolysis activity assays (Table 4) supports the idea that there is a direct

functional interaction between the distal regions of the CTR and $G\alpha_q$ which has yet to be resolved.

In summary, our PLC21 structures likely represent a snapshot of a fully inhibited PLCβ catalytic core, and when compared to the $G\alpha_q$–PLCβ3 crystal structure (Fig. 1c,d) it provides a molecular mechanism for PLCβ activation in which $G\alpha_q$ effectively sequesters an autoinhibitory motif. The mechanism is reminiscent of the action of transducin on cGMP phosphodiesterase (PDE) in the visual signal transduction cascade, wherein activated $G\alpha_t$ sequesters the inhibitory PDEγ subunit[45,46–47]. As in other canonical heterotrimeric G protein effectors, such as adenylyl cyclase[48], there are additional layers of regulation that are essential for full activity and add complexity. A better molecular understanding of how the distal regions of the CTR contribute to $G\alpha_q$ binding and enzyme activity is thus essential to composing a complete picture of how PLCβ activity is controlled and how synergy can be achieved in response to the binding of multiple activators[38].

METHODS

Cloning, expression, and purification of human PLCβ3 proteins

DNAs encoding N-terminally His-tagged human PLCβ3 (amino acids 10–1234)[49] and C-terminally truncated variants were cloned into pFastBac Dual (Invitrogen). Point mutations were introduced using QuikChange Site-Directed Mutagenesis (Stratagene) and confirmed by sequencing over the entire open reading frame. Baculovirus-infected High Five insect cells were resuspended in 20 mM HEPES pH 8, 200 mM NaCl, 10 mM β-mercaptoethanol (BME), 0.1 mM EDTA, 0.1 mM EGTA, and Roche EDTA-free protease inhibitor cocktail tablets. After sonication, the lysate was centrifuged and the supernatant was loaded on a Ni-NTA (Qiagen) column pre-equilibrated with buffer A (20 mM HEPES pH 8, 100 mM NaCl, 10 mM BME, 0.1 mM EGTA, and 0.1 mM EDTA). The column was washed with 10 column volumes of buffer A supplemented with 10 mM imidazole and 300 mM NaCl. PLCβ3 proteins were eluted with buffer A supplemented with 200 mM imidazole, and then concentrated and purified to homogeneity on two tandem Superdex S200 columns (GE Healthcare) equilibrated with 20 mM HEPES pH 8, 200 mM NaCl, 2 mM DTT, 0.1 mM EGTA, and 0.1 mM EDTA (Supplementary Fig. 5 online).

Expression and purification of $G\alpha_q$

Activity assays were conducted with protein expressed from cDNA encoding murine $G\alpha_q$ amino acids 7–359 cloned into pFastBacHTA (Invitrogen) to produce an N-terminally His_6-tagged protein. FCPIA was performed with a $G\alpha_{i/q}$ chimera in which the wild-type N-terminal helix of murine $G\alpha_q$ was replaced with $G\alpha_i$, as described previously[50]. The expression and purification protocols for both $G\alpha_q$ variants are identical. Protein expression in High Five cells was increased upon co-infection of virus encoding Ric8A–GST[51]. The cell pellet was resuspended in 20 mM HEPES pH 8, 100 mM NaCl, 10 mM BME, 3 mM $MgCl_2$, 10 μM GDP, 0.1 mM EDTA and protease inhibitors. After sonication, the lysate was centrifuged and the supernatant was loaded on a Ni-NTA (Qiagen) column. The column was washed with 20 column volumes of buffer B (20 mM HEPES pH 8, 100 mM NaCl, 10 mM BME, 1 mM $MgCl_2$, 10 μM GDP), followed by 20 column volumes of buffer B

supplemented with 10 mM imidazole and 300 mM NaCl. $G\alpha_q$ was eluted with buffer B supplemented with 150 mM imidazole. The sample was dialyzed to lower the NaCl concentration and applied to a MonoQ column. $G\alpha_q$ was eluted in 20 mM HEPES pH 8, 1 mM $MgCl_2$, 10 μM GDP, and 1 mM DTT with a gradient ranging from 0–500 mM NaCl. Peak fractions were further purified on tandem S200 columns equilibrated in 20 mM HEPES pH 8, 100 mM NaCl, 1 mM $MgCl_2$, 10 μM GDP, and 1 mM DTT.

Crystallization and structure determination

Endogenous *S*PLC21 and *L*PLC21 were purified from enucleated eye cups as described previously[16]. Full-length protein was further purified by gel filtration in 20 mM HEPES pH 8, 200 mM NaCl, and 2 mM DTT. Protein was supplemented with 5 mM $CaCl_2$ and crystallized by the hanging drop method using a 1:1 mixture of 11 mg mL^{-1} protein and well solution containing 100 mM Bis-Tris pH 7, 100–300 mM NaCl, and 20–35% (w/v) PEG 3350. Diffraction data was collected at the Advanced Photon Source at LS-CAT beam line 21-ID-F from crystals maintained at 110 K using a wavelength of 0.979 Å and initial phases were derived by molecular replacement using the human PLCβ2 (PDB entry 2ZKM) structure[22] as a search model.

Thermostability measurements

Melting temperatures **(**T_m**)** were determined by monitoring 1-anilinonaphthalene-8-sulfonic acid (ANS) binding to PLCβ3 variants during protein unfolding[52]. Wild type PLCβ3 and variants (0.3 mg mL^{-1}) were incubated with 200 μm ANS in a total volume of 5 μL in triplicate in ABgene 384-well PCR microtiter plates (Thermo-Fisher). Fluorescence was measured as the temperature was increased from 20–80 °C in 1 °C intervals using a ThermoFluor 384-well plate reader (Johnson & Johnson).

PLCβ3 activity assays

PLCβ3 basal activity and $G\alpha_q$-mediated activation was quantified by measuring the rate of hydrolysis of [^{3}H]-labeled PIP_2 in a liposome-based assay as previously described[16,53]. Briefly, lipid vesicles containing 200 μM phosphatidyl--ethanolamine, 50 μM PIP_2, and ~4000–8000 cpm [^{3}H]-labeled PIP_2 per assay were mixed, dried under nitrogen, and resuspended by sonication in 50 mM HEPES pH 7, 80 mM KCl, 2 mM EGTA, and 1 mM DTT. PLCβ3 activity was assayed at 30 °C in 50 mM HEPES pH 7, 80 mM KCl, 15 mM NaCl, 0.83 mM $MgCl_2$, 3 mM DTT, 1 mg mL^{-1} BSA, 2.5 mM EGTA, 0.2 mM EDTA with ~200 nM free Ca^{2+}. Control reactions contained the same components, but lacked free Ca^{2+}. Reactions were terminated by addition of BSA and 10% (w/v) ice-cold trichloroacetic acid. After centrifugation, free [^{3}H]-IP_3 in the supernatant was measured by scintillation counting[16,53]. To measure $G\alpha_q$-stimulated activity, purified $G\alpha_q$ was activated with 50 mM HEPES pH 7, 80 mM KCl, 30 mM NaCl, 3 mM DTT, 10 mM NaF, 20 μM $AlCl_3$, 50 μM GDP and 1.83 mM $MgCl_2$ for 30 min on ice. Increasing amounts of activated $G\alpha_q$ were added to PLCβ3 proteins, and reactions initiated by addition of liposomes, and terminated after incubation at 30 °C for 5 min.

FCPIA

The **(**R872A L876A L879A) triple mutant of PLCβ3-Δ892, which was considered to be the least likely to be autoinhibited by Hα2′, was fluorescently labeled with AlexaFluor-488 (AF488) C_5-maleimide. $G\alpha_{i/q}$ was biotinylated and linked to streptavidin coated beads as previously described[34]. Unlabeled PLCβ3 variants were added at increasing concentrations to bead-bound $G\alpha_{i/q}$, followed by addition of the AF488-labeled PLCβ3-Δ892 variant at its measured K_D (20.5 nM). The resulting mixtures were incubated for 1 hr, and then analyzed in duplicate with an Accuri C6 Flow Cytometer. Competition data was fit by nonlinear regression using a variable slope fit (PLCβ3 and mutants) or standard slope (other variants) using GraphPad Prism (version 5.0a). K_I values were estimated from fitted IC_{50} values using the Cheng-Prussof equation.

Statistical methods

Statistical analyses used ANOVA with a Dunnett's post-test as implemented in GraphPad Prism (version 5.0a).

Additional and more detailed methods are provided in the Supplementary Methods online.

Supplementary Material

Refer to Web version on PubMed Central for supplementary material.

ACKNOWLEDGMENTS

We thank Dr. Elliott Ross (University of Texas Southwestern Medical Center at Dallas) for the vector encoding human PLCβ3, and Dr. Greg Tall (University of Rochester) for the baculovirus vector expressing GST-Ric8A and insight into how to increase yields of $G\alpha_q$ before publication of his work. We also thank Dr. Peter Backlund, Section on Mass Spectrometry and Metabolism (NICHD) for mass spectrometry of PLC21 samples. This work was supported by National Institutes of Health grants HL071818 and HL086865 (J.J.G.T.), and by the Intramural Research program of the National Institute on Deafness and Other Communication Disorders, National Institutes of Health (J.K.N.). Our research used the Cell and Molecular Biology Core of the Michigan Diabetes Research and Training Center supported by DK20572. Use of the Advanced Photon Source was supported by the U. S. Department of Energy, Office of Science, Office of Basic Energy Sciences, under Contract No. DE-AC02-06CH11357. Use of the LS-CAT Sector 21 was supported by the Michigan Economic Development Corporation and the Michigan Technology Tri-Corridor for the support of this research program (Grant 085P1000817).

REFERENCES

1. Rhee SG. Regulation of phosphoinositide-specific phospholipase C. Annu Rev Biochem. 2001; 70:281–312. [PubMed: 11395409]
2. Rebecchi MJ, Pentyala SN. Structure, function, and control of phosphoinositide-specific phospholipase C. Physiol Rev. 2000; 80:1291–1335. [PubMed: 11015615]
3. Taylor SJ, Exton JH. Two a subunits of the G_q class of G proteins stimulate phosphoinositide phospholipase C-β1 activity. FEBS Lett. 1991; 286:214–216. [PubMed: 1650713]
4. Smrcka AV, Hepler JR, Brown KO, Sternweis PC. Regulation of polyphosphoinositide-specific phospholipase C activity by purified G_q. Science. 1991; 251:804–807. [PubMed: 1846707]
5. Park D, Jhon DY, Lee CW, Lee KH, Rhee SG. Activation of phospholipase C isozymes by G protein βγ subunits. J Biol Chem. 1993; 268:4573–4576. [PubMed: 8383116]
6. Boyer JL, Waldo GL, Harden TK. βγ-subunit activation of G-protein-regulated phospholipase C. J Biol Chem. 1992; 267:25451–25456. [PubMed: 1460039]

7. Smrcka AV, Sternweis PC. Regulation of purified subtypes of phosphatidylinositol-specific phospholipase C β by G protein α and βγ subunits. J Biol Chem. 1993; 268:9667–9674. [PubMed: 8387502]
8. Sternweis PC, Smrcka AV. G proteins in signal transduction: the regulation of phospholipase C. Ciba Found Symp. 1993; 176:96–106. discussion 106–11. [PubMed: 8299429]
9. Illenberger D, et al. Stimulation of phospholipase C-β2 by the Rho GTPases Cdc42Hs and Rac1. EMBO J. 1998; 17:6241–6249. [PubMed: 9799233]
10. Harden TK, Hicks SN, Sondek J. Phospholipase C isozymes as effectors of Ras superfamily GTPases. J Lipid Res. 2009; 50(Suppl):S243–S248. [PubMed: 19033212]
11. Sugden PH, Clerk A. Cellular mechanisms of cardiac hypertrophy. J Mol Med. 1998; 76:725–746. [PubMed: 9826118]
12. Berridge MJ. Cardiac calcium signalling. Biochem Soc Trans. 2003; 31:930–933. [PubMed: 14505451]
13. Ju H, Zhao S, Tappia PS, Panagia V, Dixon IM. Expression of $G_q\alpha$ and PLC-β in scar and border tissue in heart failure due to myocardial infarction. Circulation. 1998; 97:892–899. [PubMed: 9521338]
14. Woodcock EA, Kistler PM, Ju Y-K. Phosphoinositide signalling and cardiac arrhythmias. Cardiovasc. Res. 2009; 82:286–295. [PubMed: 18940816]
15. Schneuwly S, Burg MG, Lending C, Perdew MH, Pak WL. Properties of photoreceptor-specific phospholipase C encoded by the norpA gene of Drosophila melanogaster. J Biol Chem. 1991; 266:24314–24319. [PubMed: 1662208]
16. Mitchell J, Gutierrez J, Northup JK. Purification, characterization, and partial amino acid sequence of a G protein-activated phospholipase C from squid photoreceptors. J Biol Chem. 1995; 270:854–859. [PubMed: 7822322]
17. Shortridge RD, et al. A Drosophila phospholipase C gene that is expressed in the central nervous system. J Biol Chem. 1991; 266:12474–12480. [PubMed: 2061323]
18. Essen LO, et al. Structural mapping of the catalytic mechanism for a mammalian phosphoinositide-specific phospholipase C. Biochemistry. 1997; 36:1704–1718. [PubMed: 9048554]
19. Ellis MV, et al. Catalytic domain of phosphoinositide-specific phospholipase C (PLC). Mutational analysis of residues within the active site and hydrophobic ridge of PLCδ1. J Biol Chem. 1998; 273:11650–11659. [PubMed: 9565585]
20. Suh PG, et al. Multiple roles of phosphoinositide-specific phospholipase C isozymes. BMB Rep. 2008; 41:415–434. [PubMed: 18593525]
21. Jezyk MR, et al. Crystal structure of Rac1 bound to its effector phospholipase C-β2. Nat Struct Mol Biol. 2006; 13:1135–1140. [PubMed: 17115053]
22. Hicks SN, et al. General and versatile autoinhibition of PLC isozymes. Mol Cell. 2008; 31:383–394. [PubMed: 18691970]
23. Waldo GL, et al. Kinetic Scaffolding mediated by a phospholipase C-β and G_q signaling complex. Science. 2010; 330:974–980. [PubMed: 20966218]
24. Zhang W, Neer EJ. Reassembly of phospholipase C-β2 from separated domains: analysis of basal and G protein-stimulated activities. J Biol Chem. 2001; 276:2503–2508. [PubMed: 11044443]
25. Schnabel P, Camps M. Activation of a phospholipase Cβ2 deletion mutant by limited proteolysis. Biochem J. 1998; 330(Pt 1):461–468. [PubMed: 9461544]
26. Ilkaeva O, Kinch LN, Paulssen RH, Ross EM. Mutations in the carboxyl-terminal domain of phospholipase C-β1 delineate the dimer interface and a potential $G\alpha_q$ interaction site. J Biol Chem. 2002; 277:4294–4300. [PubMed: 11729196]
27. Kim CG, Park D, Rhee SG. The role of carboxyl-terminal basic amino acids in $G_q\alpha$-dependent activation, particulate association, and nuclear localization of phospholipase C-β1. J Biol Chem. 1996; 271:21187–21192. [PubMed: 8702889]
28. Park D, Jhon DY, Lee CW, Ryu SH, Rhee SG. Removal of the carboxyl-terminal region of phospholipase C-β1 by calpain abolishes activation by $G\alpha_q$. J Biol Chem. 1993; 268:3710–3714. [PubMed: 8429045]

29. Singer AU, Waldo GL, Harden TK, Sondek J. A unique fold of phospholipase C-β mediates dimerization and interaction with $G\alpha_q$. Nat Struct Biol. 2002; 9:32–36. [PubMed: 11753430]
30. Paulssen RH, Woodson J, Liu Z, Ross EM. Carboxyl-terminal fragments of phospholipase C-β1 with intrinsic G_q GTPase-activating protein (GAP) activity. J Biol Chem. 1996; 271:26622–26629. [PubMed: 8900136]
31. Wu D, Jiang H, Katz A, Simon MI. Identification of critical regions on phospholipase C-β1 required for activation by G-proteins. J Biol Chem. 1993; 268:3704–3709. [PubMed: 8381437]
32. Koyanagi M, Ono K, Suga H, Iwabe N, Miyata T. Phospholipase C cDNAs from sponge and hydra: antiquity of genes involved in the inositol phospholipid signaling pathway. FEBS Lett. 1998; 439:66–70. [PubMed: 9849879]
33. Jhon DY, et al. Cloning, sequencing, purification, and G_q-dependent activation of phospholipase C-β3. J Biol Chem. 1993; 268:6654–6661. [PubMed: 8454637]
34. Shankaranarayanan A, et al. Assembly of high order $G\alpha_q$-effector complexes with RGS proteins. J Biol Chem. 2008; 283:34923–34934. [PubMed: 18936096]
35. Gu S, et al. Unique hydrophobic extension of the RGS2 amphipathic helix domain imparts increased plasma membrane binding and function relative to other RGS R4/B subfamily members. J Biol Chem. 2007; 282:33064–33075. [PubMed: 17848575]
36. Hepler JR, et al. Purification from Sf9 cells and characterization of recombinant $G_q\alpha$, $G_{11}\alpha$.Activation of purified phospholipase C isozymes by Gα subunits. J Biol Chem. 1993; 268:14367–14375. [PubMed: 8314796]
37. Lee SB, Shin SH, Hepler JR, Gilman AG, Rhee SG. Activation of phospholipase C-β2 Mutants by G Protein α_q, βγ Subunits. J. Biol. Chem. 1993; 268:25952–25957. [PubMed: 8245028]
38. Philip F, Kadamur G, Silos RG, Woodson J, Ross EM. Synergistic activation of phospholipase C-β3 by $G\alpha_q$ and Gβγ describes a simple two-state coincidence detector. Curr Biol. 2010; 20:1327–1335. [PubMed: 20579885]
39. Woodcock EA, et al. Selective activation of the "b" splice variant of phospholipase Cβ1 in chronically dilated human and mouse atria. J Mol Cell Cardiol. 2009; 47:676–683. [PubMed: 19729020]
40. Achour L, Labbe-Jullie C, Scott MG, Marullo S. An escort for GPCRs: implications for regulation of receptor density at the cell surface. Trends Pharmacol Sci. 2008; 29:528–535. [PubMed: 18760490]
41. Jenco JM, Becker KP, Morris AJ. Membrane-binding properties of phospholipase C-β1 and phospholipase C-β2: role of the C-terminus and effects of polyphosphoinositides, G-proteins and Ca^{2+} Biochem J. 1997; 327(Pt 2):431–437. [PubMed: 9359412]
42. Anderson CM, Zucker FH, Steitz TA. Space-filling models of kinase clefts and conformation changes. Science. 1979; 204:375–380. [PubMed: 220706]
43. Daniel RM. The upper limits of enzyme thermal stability. Enzyme and Microbial Technology. 1996; 19:74–79.
44. Wu D, Katz A, Simon MI. Activation of phospholipase Cβ2 by the α and βγ subunits of trimeric GTP-binding protein. Proc Natl Acad Sci U S A. 1993; 90:5297–5301. [PubMed: 8389480]
45. Hurley JB. Molecular properties of the cGMP cascade of vertebrate photoreceptors. Annu Rev Physiol. 1987; 49:793–812. [PubMed: 3032082]
46. Slep KC, et al. Structural determinants for regulation of phosphodiesterase by a G protein at 2.0 Å. Nature. 2001; 409:1071–1077. [PubMed: 11234020]
47. Arshavsky VY, Lamb TD, Pugh EN Jr. G proteins and phototransduction. Annu Rev Physiol. 2002; 64:153–187. [PubMed: 11826267]
48. Sunahara RK, Taussig R. Isoforms of mammalian adenylyl cyclase: multiplicities of signaling. Mol Interv. 2002; 2:168–184. [PubMed: 14993377]

METHODS ONLY REFERENCES

49. Biddlecome GH, Berstein G, Ross EM. Regulation of phospholipase C-β1 by G_q and m_1 muscarinic cholinergic receptor. Steady-state balance of receptor-mediated activation and GTPase-

activating protein-promoted deactivation. J Biol Chem. 1996; 271:7999–8007. [PubMed: 8626481]

50. Tesmer VM, Kawano T, Shankaranarayanan A, Kozasa T, Tesmer JJ. Snapshot of activated G proteins at the membrane: the $G\alpha_q$-GRK2-$G\beta\gamma$ complex. Science. 2005; 310:1686–1690. [PubMed: 16339447]
51. Chan P, et al. Purification of heterotrimeric G protein α subunits by GST-Ric-8 association: primary characterization of purified $G\alpha_{olf}$. J Biol Chem. 2011; 286:2625–2635. [PubMed: 21115479]
52. Mezzasalma TM, et al. Enhancing recombinant protein quality and yield by protein stability profiling. J Biomol Screen. 2007; 12:418–428. [PubMed: 17438070]
53. Ghosh M, Smrcka AV. Assay for G protein-dependent activation of phospholipase Cβ using purified protein components. Methods Mol Biol. 2004; 237:67–75. [PubMed: 14501039]

METHODS ONLY REFERENCES

49. Biddlecome GH, Berstein G, Ross EM. Regulation of phospholipase C-β1 by G_q and m_1 muscarinic cholinergic receptor. Steady-state balance of receptor-mediated activation and GTPase-activating protein-promoted deactivation. J Biol Chem. 1996; 271:7999–8007. [PubMed: 8626481]
50. Tesmer VM, Kawano T, Shankaranarayanan A, Kozasa T, Tesmer JJ. Snapshot of activated G proteins at the membrane: the $G\alpha_q$-GRK2-$G\beta\gamma$ complex. Science. 2005; 310:1686–1690. [PubMed: 16339447]
51. Chan P, et al. Purification of heterotrimeric G protein α subunits by GST-Ric-8 association: primary characterization of purified $G\alpha_{olf}$. J Biol Chem. 2011; 286:2625–2635. [PubMed: 21115479]
52. Mezzasalma TM, et al. Enhancing recombinant protein quality and yield by protein stability profiling. J Biomol Screen. 2007; 12:418–428. [PubMed: 17438070]
53. Ghosh M, Smrcka AV. Assay for G protein-dependent activation of phospholipase Cβ using purified protein components. Methods Mol Biol. 2004; 237:67–75. [PubMed: 14501039]

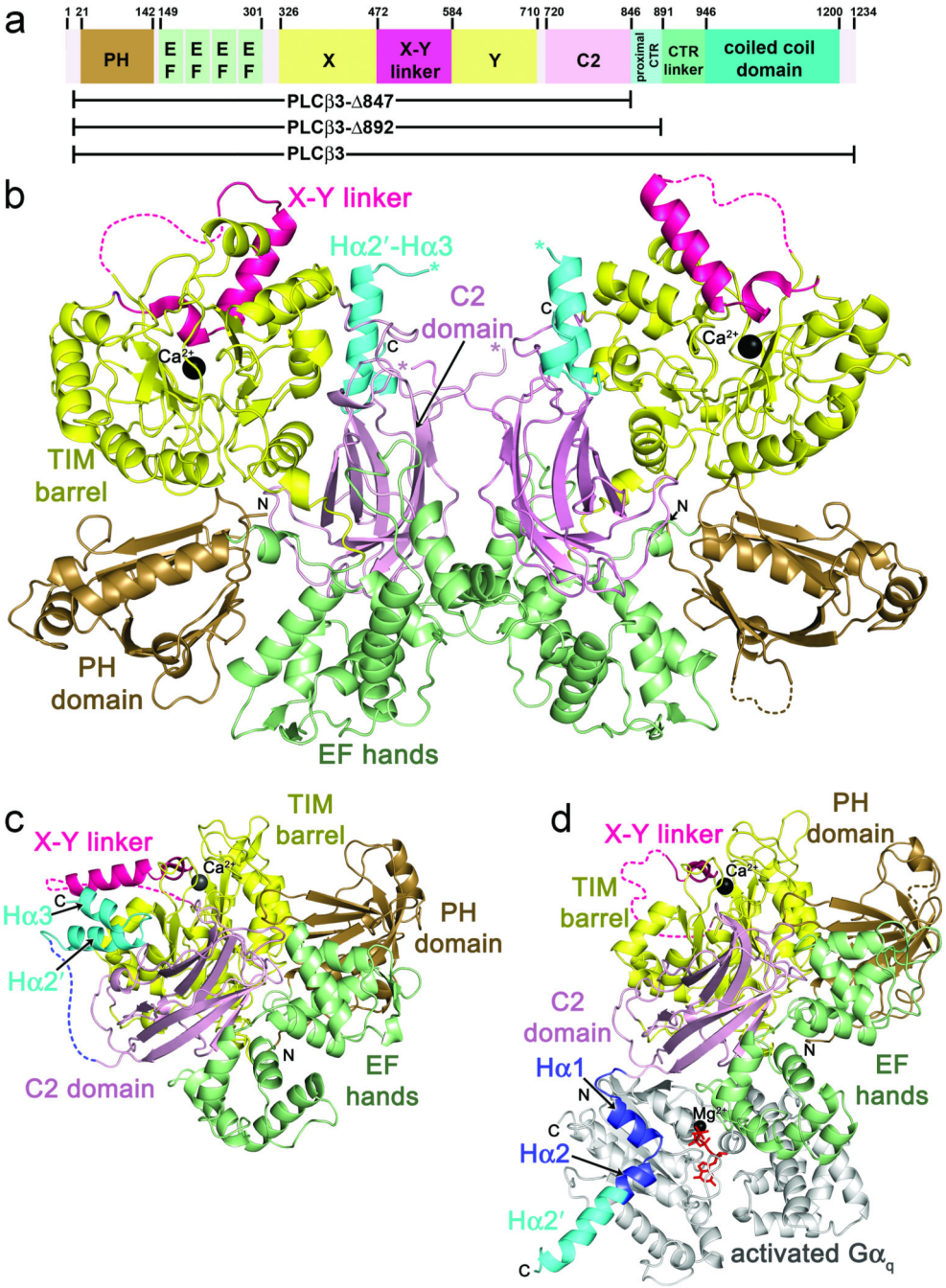

Figure 1.

Primary and tertiary structures of PLCβ family members, and comparison of cephalopod PLC21 with the $G\alpha_q$–PLCβ3 complex. (**a**) Primary structure of human PLCβ3. PLCβ3 truncations used in this paper are indicated below the diagram. Numbers above the diagram correspond to amino acid positions at domain boundaries. (**b**) Crystal structure of *L*PLC21. *L*PLC21 crystallized as a dimer with pseudo two-fold symmetry. Domains are colored as in ***a***. The Hα2′-Hα3 hairpin from the proximal CTR is shown in cyan, and the catalytic Ca^{2+} is shown as a black sphere. Disordered loops are drawn as dashed lines, with the exception of

the connection between the C2 domain and the beginning of Hα2′, which is ambiguous in the dimer interface. The C-terminus of the C2 domain and start of Hα2′ are marked with pink and blue asterisks, respectively. N- and C-terminal ends of the protein fragment resolved in the crystal structure are labeled N and C, respectively. (**c**) Crystal structure of *S*PLC21. Domains are colored as in ***b***. (**d**) Crystal structure of the $G\alpha_q$–PLCβ3 complex (PDB entry 3OHM)[23]. Hα1 and Hα2, which form the primary $G\alpha_q$ binding site, are shown in dark blue. Residues corresponding to Hα2′ in the PLC21 structures are shown in cyan. Activated $G\alpha_q$ is shown in light gray, with GDP and AlF_4 colored red, and Mg^{2+} black.

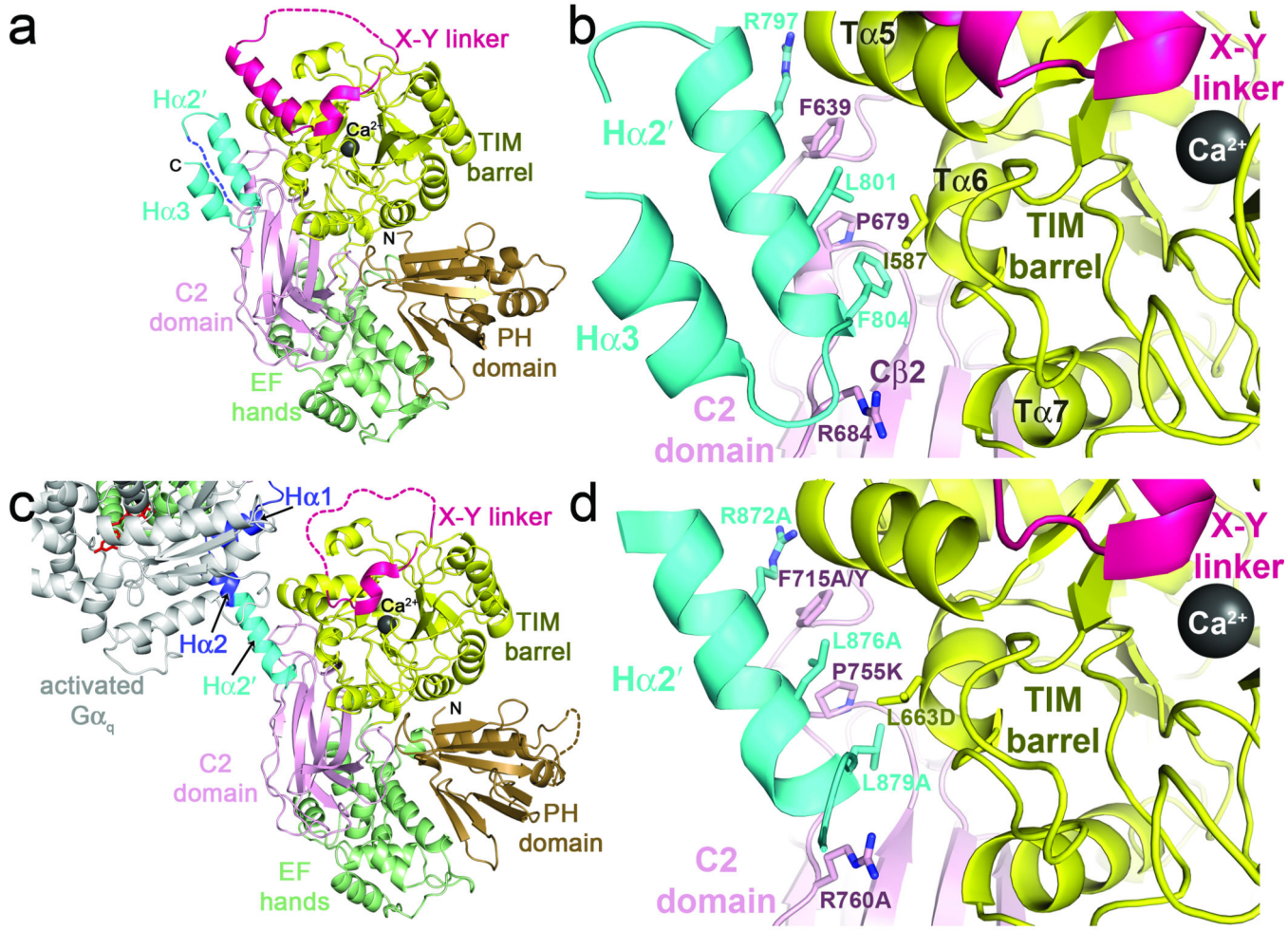

Figure 2.

Interactions of Hα2′ with the catalytic core. (**a**) The *S*PLC21 Hα2′ helix docks in a conserved cleft formed between the TIM barrel and C2 domains, in close proximity to the active site and the X–Y linker. The shorter Hα3 helix forms a hairpin interaction with Hα2′ stabilized by hydrophobic interactions. Domains are colored as in ***1a***. (**b**) Specific interactions of *S*PLC21 Hα2′ with the catalytic core. Side chains that make large contributions to the binding interface are shown as sticks with carbons colored according to their respective domains and nitrogens blue. (**c**) The Hα2′-catalytic core interaction is recapitulated in a crystal contact of the $G\alpha_q$–PLCβ3 structure (PDB entry 3OHM)[23]. Domains are colored as in ***1d***. The subunit of $G\alpha_q$ shown is in complex with a different catalytic core in the crystal lattice. (**d**) Specific interactions between Hα2′ and the catalytic core in human PLCβ3 (Fig. 1c). Residues analogous to those of *S*PLC21 shown in ***b*** are drawn as sticks, and site-directed mutations created in this study to perturb the interface are indicated. The *S*PLC21 Hα2′ helix is continuous, whereas Hα2′ in human PLCβ3 is kinked at Ala877, as if to optimize the interactions of the Leu879 side chain, which is smaller than that of the corresponding Phe804 residue in *S*PLC21.

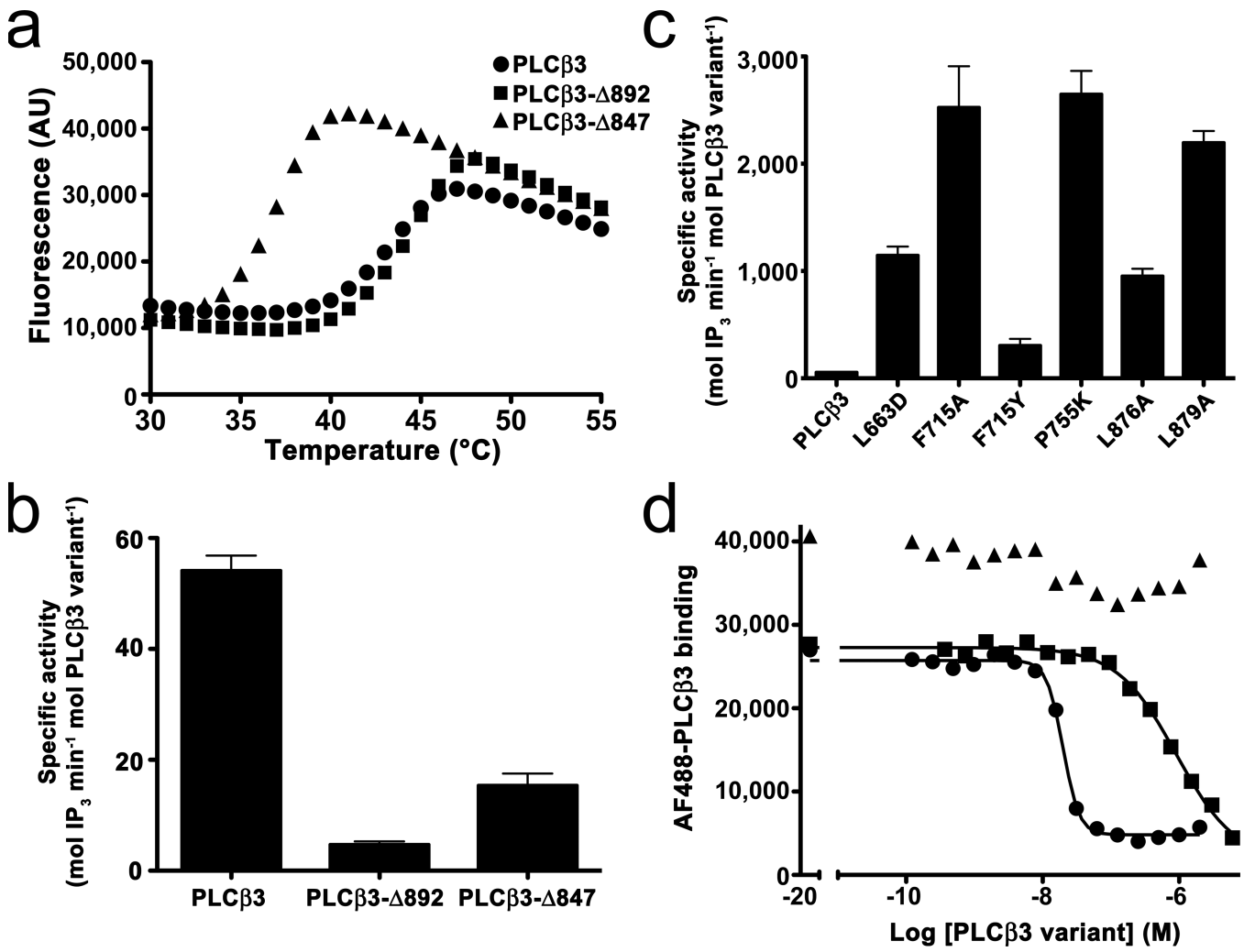

Figure 3.

Functional studies of PLCβ3 variants. (**a**) The proximal CTR stabilizes the catalytic core. ThermoFluor assays were used to measure the melting point of three PLCβ3 variants by monitoring the change in fluorescence of ANS. Representative curves are shown for PLCβ3 (circles), PLCβ3-Δ892 (squares), and PLCβ3-Δ847 (triangles). PLCβ3-Δ847 is 5–7 °C less stable (left-shifted) than PLCβ3 or PLCβ3-Δ892. See Supplementary Table 1. AU, arbitrary units. (**b**) Comparison of the basal activity of PLCβ3 variants. Deletion of the proximal CTR in PLCβ3-Δ847 increases basal activity relative to PLCβ3-Δ892. The higher basal activity of PLCβ3 reflects the contribution of more distal regions of the CTR to maximal activity. Activity was measured by counting free [^{3}H]-IP_3 released from liposomes containing [^{3}H]-PIP_2 at 30 °C in the presence of ~200 nM free Ca^{2+} at 4–5 time points. The data shown represent at least four individual experiments performed in duplicate ± SEM. (**c**) Mutation of PLCβ3 at positions that contribute to the Hα2′-catalytic core interface dramatically increase basal activity, indicating that this interaction is involved in autoinhibition. (**d**) Distal regions of the PLCβ3 CTR enhance binding to $G\alpha_q$. FCPIA was used to quantify the ability of PLCβ3 truncations to displace AlexaFluor488-labeled PLCβ3-Δ892 (R872A L876A L879A triple mutant) from biotinylated, AlF_4-activated $G\alpha_{i/q}$ bound to avidin beads. Representative

curves for PLCβ3 (circles), PLCβ3-Δ892 (squares) and PLCβ3-Δ847 (triangles) are shown. See Table 3 for measured inhibition constants.

Table 1

Data collection and refinement statistics

	***Sepia* PLC21**	***Loligo* PLC21**
Data collection		
Space group	$P2_12_12_1$	$P2_12_12_1$
Cell dimensions		
a, *b*, *c* (Å)	60.8, 83.4, 163.1	82.4, 148.9, 151.6
α, *β*, *γ* (°)	90, 90, 90	90, 90, 90
Resolution (Å)	27.4-2.00 (2.04-2.00)*	29.97-3.10 (3.15-3.10)
R_{sym} or R_{merge}	0.069 (0.679)	0.146 (0.814)
I / σI	17.4 (1.58)	14.2 (2.3)
Completeness (%)	97.7 (98.2)	100 (100)
Redundancy	3.7 (3.6)	7.2 (7.2)
Refinement		
Resolution (Å)	27.4-2.00	30.0-3.20
No. reflections	53335	29832
R_{work} / R_{free}	0.176/0.208	0.232/0.256
No. atoms		
Protein	12668	24953
Ligand/ion	126	2
Water	452	38
B-factors		
Protein	20.2	61.5
Ligand/ion	45.9	60.2
Water	28.1	36.3
R.m.s. deviations		
Bond lengths (Å)	0.006	0.006
Bond angles (°)	0.946	0.881

Each data set was collected from a single crystal.

*Values in parentheses are for highest-resolution shell.

Table 2

Basal Activity of PLCβ3 Variants

Variant	Specific Activity ± SEM[a] (mol IP_3 min^{-1} mol^{-1}PLCβ3)	Fold Increase Relative to Wild-Type
PLCβ3 (wt)[b]	54 ± 2.7	1
-L663D	1150 ± 81	23
-F715A	2500 ± 380	51
-F715Y	310 ± 62	6
-P755K	2650 ± 216	53
-L876A	950 ± 69	19
-L879A	2000 ± 190	41
PLCβ3-Δ892 (wt)	4.7 ± 0.6	1
-F715A[b]	9.5 ± 0.4	2
-R760A[b]	7.2 ± 0.7	2
-R872A[b]	22 ± 2.2	5
-L876A	9.9 ± 1.6	2
-L879A[b]	13 ± 1.9	3
-L876A L879A[b]	14 ± 1.1	3
-AAA[b,c]	14 ± 1.4	3
PLCβ3-Δ847 (wt)[b]	15 ± 2.1	1
-F715A	39 ± 4.4	2.3

[a] At least five independent experiments performed in duplicate.

[b] Includes samples from at least two independent protein purifications.

[c] R872A L876A L879A

Table 3

Inhibition Constants of PLCβ3 Variants Measured by FCPIA

Variant	K_I ± SEM (nM) (n)[a]
PLCβ3 (wt)[b]	6.0 ± 1. (5)
-F715A	2.0 ± 0.3 (4)
-L876A	3.1 ± 0.5 (4)
-L879A	1.6 ± 0.1 (3)
PLCβ3-Δ892 (wt)[b]	270 ± 60 (4)
-F715A[b]	31 ± 6 (3)
-AAA[c]	26 ± 6 (3)
PLCβ3-Δ847 (wt)[b]	NB[d] (3)

[a] Number (n) of independent experiments performed in duplicate.

[b] Includes samples from at least two independent protein purifications.

[c] R872A L876A L879A

[d] No binding detected.

Table 4

$G\alpha_q$ Activation of PLCβ3 Variants *in Vitro*[a]

Variant	EC_{50} (nM)	Increase in Activity (mol IP_3 min^{-1} mol^{-1}PLCβ3)	Fold Max. Activity Over Basal[b]
PLCβ3 (wt)	3.2 ± 0.6	1100 ± 100	21
-F715A	9.7 ± 1.4	5000 ± 690	3.0
-P755K	10. ± 1.8	3200 ± 230	2.2
-L876A	0.7 ± 0.1	1360 ± 120	2.4
-L879A	9.4 ± 1.7	4700 ± 310	3.3
-AAA[c]	ND[d]	ND	ND
PLCβ3-Δ892 (wt)	130 ± 19	30 ± 4	7.3
-F715A	54 ± 13	41 ± 3	3.9
-AAA[c]	67 ± 13	33 ± 2	3.3
PLCβ3-Δ847 (wt)	---	−9 ± 2	0.4

[a] Three to 12 independent experiments, each performed in duplicate, ± SEM. See Supplementary Figure 4 online.

[b] Fold activation is calculated as the (basal activity + increase in activity) × basal activity^{-1}. Due to errors in determining very low basal activities in these dose response curves, basal activities are taken from Table 2.

[c] R872A L876A L879A

[d] Not determined. The full-length version of this protein was highly susceptible to proteolytic cleavage after the proximal CTR, and consequently the activity could not be unambiguously measured.